

LES Modelling of Obstacles-Accelerated Premixed Flames

Valeria Di Sarli¹, Almerinda Di Benedetto² and Gennaro Russo¹

¹Dipartimento di Ingegneria Chimica, Università degli Studi di Napoli “Federico II”,
Piazzale Tecchio 80, 80125, Napoli, Italy

²Istituto di Ricerche sulla Combustione, CNR, Via Diocleziano 328, 80124, Napoli,
Italy

In gas explosions, the acceleration of a flame front and the consequent overpressure are intensified as a result of the coupling between the moving flame and the turbulence induced by the presence of local blockage in the flame path.

In the present paper a validated CFD model based on the advanced Large Eddy Simulation (LES) approach was adopted to study the unsteady propagation of stoichiometric CH₄/air premixed flame around an obstacle in a vented chamber initially filled with quiescent mixture. A sub-grid combustion model was implemented which takes into account the interaction between reaction rate and flow field, following all the stages of flame propagation from laminar to fully turbulent. Simulations were also run by assuming the flame speed equal to the laminar value during all the propagation time, by eliminating the obstruction in the chamber, and by assuming laminar propagation in the empty chamber. From the comparison of the results obtained, it turns out that the competition between combustion rate and venting rate is the main mechanism affecting both, number and intensity of the overpressure peaks observed.

1. Introduction

Gas explosions almost always occur under conditions having disturbing elements present in the path of the propagating flame. The coupling of the moving flame front and the turbulent flow field induced by the local blockage enhances the flame acceleration and the subsequent overpressure.

In the last years, thanks to the progress made in the field of experimental diagnostics, highly resolved data related to the unsteady interaction between premixed flames and obstacles have been obtained in terms of flame images and speed profiles, flow field vectors and turbulence characteristics maps (Lindstedt and Sakthitharan, 1998; Ibrahim et al., 2001; Hargrave et al., 2002; Patel et al., 2003; Jarvis and Hargrave, 2006). These works have enabled a basic understanding of the development details of flames propagating in small-scale explosion chambers starting from quiescent conditions.

On the theoretical side, the adoption of CFD models has allowed the opportunity of simulating explosions in presence of obstacles taking into account the full coupling of flow, turbulence and combustion by means of both, RANS modelling (Naamansen et al., 2002; Patel et al., 2003) and the more sophisticated Large Eddy Simulation (LES) approach (Kirkpatrick et al., 2003; Di Sarli et al., 2007).

Highly resolved experimental data are useful also to validate detailed CFD models which, in turn, may allow identifying each mechanism responsible for the pressure rise, thus evaluating its contribution by varying conditions and parameters.

In a previous work we have proposed a LES-based model to study the unsteady propagation of stoichiometric CH₄/air premixed flame around an obstacle in a vented combustion chamber initially filled with quiescent mixture (Di Sarli et al., 2007). The numerical predictions were compared against the experimental data by Ibrahim et al. (2001), resulting in a good agreement in terms of overpressure time history, flame speed profile along the chamber and global features of flame propagation. The model results have shown that the mechanism responsible for the overpressure peaks observed is the competition between combustion rate and venting rate which establishes in the chamber zones upstream and downstream of the obstacle.

In the present paper these conclusions are examined comparing our previous results with those from simulations run with the same model, but (i) by assuming the flame speed equal to the laminar value during the whole propagation (thus decoupling the flame-turbulence interaction), (ii) by eliminating the obstacle in the chamber (thus focusing on the venting effect) and (iii) by assuming laminar propagation in the empty chamber (thus having a reference case of laminar propagation without the obstacle).

2. The model

The LES model adopted to simulate the unsteady propagation of stoichiometric CH₄/air flame around obstacles has been described in our previous work (Di Sarli et al., 2007).

Briefly, the employed model equations were obtained by Favre-filtering the governing equations for compressible flow with premixed combustion. Turbulence closure was achieved using the dynamic Smagorinsky model (Lilly, 1992). Chemical reaction at the sub-grid scale was parameterized according to the flame surface density approach (Boger et al., 1998). The flame surface density was expressed as function of the sub-grid scale flame wrinkling factor (i.e., the projection of the sub-grid scale surface in the propagating direction), Ξ_Δ , taking into account the coupling of unresolved turbulence and reaction rate (Charlette et al., 2002). For the corrugated flamelets and the thin reaction zones regimes the model by Charlette et al. (2002), derived from direct numerical simulations of flame/vortex interactions, was implemented. In the broken reaction zones, the global flame quenching (i.e., $\Xi_\Delta = 0$) was taken into account according to the quenching limits discussed by Meneveau and Poinso (1991).

We validated the model against the experimental data by Ibrahim et al. (2001) (Di Sarli et al., 2007). We chose as test case the experiment on the propagation of stoichiometric CH₄/air premixed flame in a closed-end chamber (75 mm x 150 mm x 450 mm) containing a 50 % blockage obstacle with a rectangular cross-section (40 mm x 12 mm). The chamber was initially filled with quiescent mixture ignited at the closed end center.

3. Results and discussion

The results here presented have been obtained from simulations run in four different conditions: test case (i.e., conditions of the experiment by Ibrahim et al., 2001) (Run A), assuming a laminar flame speed during the whole propagation (i.e., $\Xi_\Delta = 1$) (Run B), in

absence of the obstacle (Run C) and assuming a laminar propagation in the empty chamber (Run D). With Run B the flame-turbulence interaction is decoupled, thus affecting the combustion rate. With Run C we focus only on venting by removing the obstacle effects on both, flow field and flame propagation. Run D represents a reference case of laminar flame propagation in the empty chamber.

In Figure 1 the time trends of the calculated mean overpressure at the bottom end of the chamber are shown for all the simulated cases. In the early stages of flame propagation two low and smooth peaks occurs in each case (Figure 1, $t \leq 30$ ms). Starting from $t > 30$ ms, more intense peaks are found, two with Run A and three with Run B, Run C and Run D (Figure 1). These peaks are reached earlier and are higher in the test case (Run A), than in the case of empty chamber (Run C) and eventually in the fully laminar cases, with (Run B) and without the obstacle (Run D).

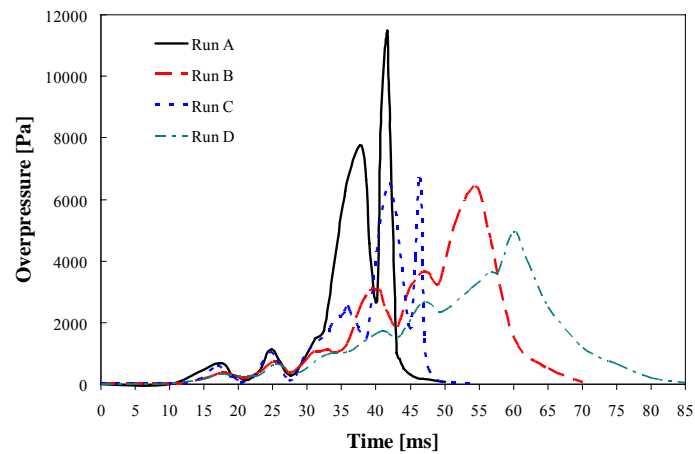


Figure 1 – Computed time histories of the mean overpressure at the bottom end of the chamber: test case (Run A); laminar propagation (Run B); empty chamber (Run C); laminar propagation in empty chamber (Run D).

The presence of overpressure peaks also in the case of laminar propagation in the empty chamber (Run D) suggests that the mechanism underlying the overpressure histories of Figure 1 has to be ascribed to a phenomenon present in all the cases simulated: the competition between combustion rate and venting rate. In order to get insight into the nature of the overpressure trends of Figure 1 it is useful to match them with the corresponding time sequences of the computed temperature maps reported in Figure 2.

The first two peaks occur about at the same times in each case: the first peak is at $t \approx 18$ ms and the second one is at $t = 25$ ms (Figure 1). Figure 2 (1st and 2nd columns) shows that at these times the flame has covered the same distances from the closed end face (i.e., the ignition face) of the chamber in all the runs: at these distances in Run A and Run B the flame is quite far from the obstacle whose presence, then, does not affect the flame propagation and the subsequent overpressure trend. During these initial stages the propagation is laminar and takes place in very similar conditions in all the cases. The corresponding oscillating behaviour of the overpressure history observed in each run (Figure 1, $t \leq 30$ ms) can be seen as a result of the coupling of the combustion rate and the venting rate with the pressure variation acting as a feedback. Indeed, starting from the ignition, the pressure increases due to the accumulation of burnt gas in the

chamber. The consequent gas compression promotes the venting rate towards the exit, which empties the chamber, thus lowering the pressure and causing the first peak (Figure 1 and Figure 2, $t \approx 18$ ms). Successively, the pressure and then the venting rate decreases and the effect of the combustion rate overcomes, thus giving rise to the second peak (Figure 1 and Figure 2, $t = 25$ ms).

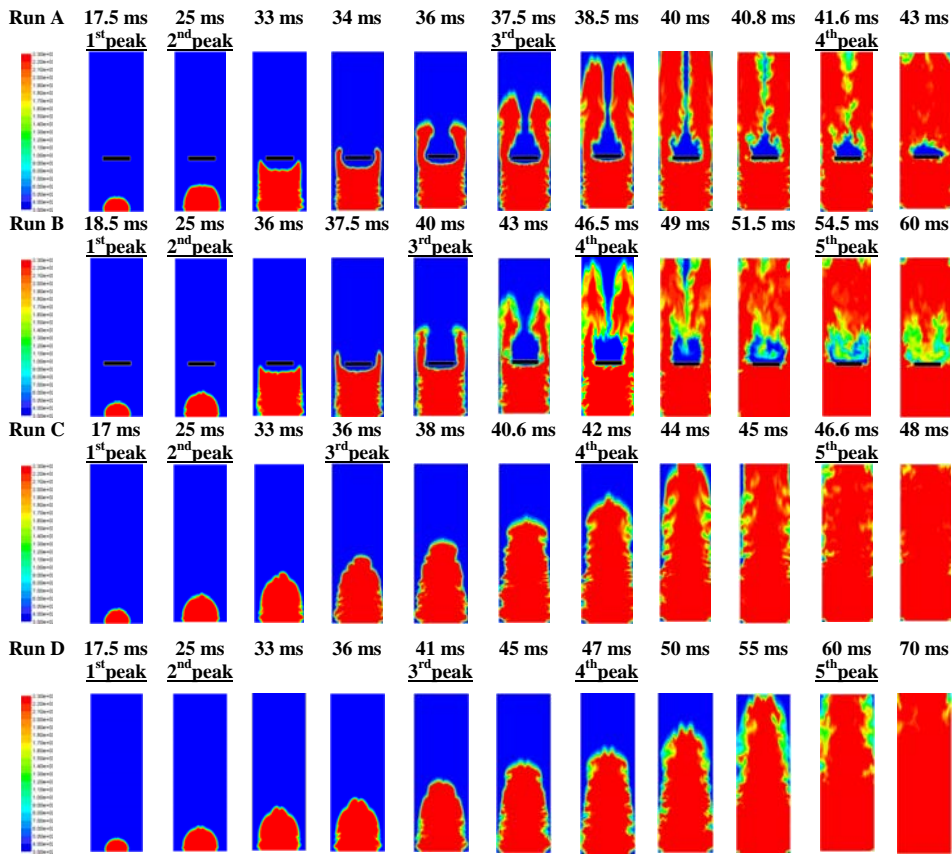


Figure 2 – Time sequences of the computed temperature maps: test case (Run A); laminar propagation (Run B); empty chamber (Run C); laminar propagation in empty chamber (Run D).

Concerning the third peak, it is found at $t = 37.5$ ms in Run A, at $t = 40$ ms in Run B, at $t = 36$ ms in Run C and at $t = 41$ ms in Run D (Figure 1). From Figure 2 it turns out that at the time of this peak the flame has reached almost the same position in the chamber in Run A and in Run B (downstream of the obstacle), and it is at about half of the entire chamber's length in both, Run C and Run D.

In a previous work we have examined the simulation results of the test case (Run A) (Di Sarli et al., 2007). We have found that when the flame reaches the obstacle, it accelerates rapidly due to two reasons (Figure 2, Run A, $t \geq 33$ ms). The first reason is linked to the flow cross-section constriction induced by the obstacle, which produces a jetting flame downstream of the obstruction. The second reason is related to the coupling with the turbulence generated around the obstacle by the interaction between

the unburnt mixture flow, pushed ahead by the propagating flame front, and the obstacle itself. In particular, the flame ranges from a laminar combustion regime (upstream of the obstacle) to a fully turbulent combustion regime (downstream of the obstacle). In these conditions, the passage between the obstacle and the chamber side walls is blocked by the flame, while unburnt mixture is still present in the zone upstream of the obstacle (Figure 2, Run A, $t = 33$ ms). Because of this *obstacle-side combustion*, the laminar propagation upstream of the obstacle almost proceeds as in a closed vessel (Figure 2, Run A, $33 \leq t \leq 37.5$ ms), thus leading to the third peak (Figure 1).

Compared to the test case (Run A), in the fully laminar case (Run B) the flame passage through the obstacle-wall gaps is slower due to the absence of the turbulence-combustion interaction and, then, the effect of the *obstacle-side combustion* is less intense. Moreover, the flame touches the obstacle later, leaving a smaller amount of unburnt mixture upstream of the obstacle (Figure 2, Run B, $36 \leq t \leq 37.5$ ms) than the test case (Figure 2, Run A, $33 \leq t \leq 34$ ms). Consequently, Run B results in a third overpressure peak that is lower than Run A (Figure 1).

In the case of empty chamber (Run C), the third peak corresponds again to an almost laminar phase of propagation, but without the obstacle effects (Figure 2, Run C, $t = 36$ ms). Then, this peak is lower than both, the third peak in Run A and the third peak in Run B (Figure 1). In Run D the propagation in absence of the obstacle is fully laminar (Figure 2, Run D, $t = 41$ ms) and, then, the third peak is the lowest one in Figure 1.

The fourth overpressure peak in the test case (Run A) is found at $t = 41.6$ ms (Figure 1). We have shown that it is linked to the explosion of the reactants trapped behind the obstacle (Figure 2, Run A, $40 \leq t \leq 43$ ms) (Di Sarli et al., 2007). In particular, this *over-combustion* occurs in conditions of almost stopped venting, as the flame exits from the chamber and gives rise to an *external explosion*.

In the fully laminar case with the obstacle (Run B), after the third peak the combustion downstream of the obstruction produces one peak more than the test case (Run A) (Figure 1 and Figure 2, Run B, $43 \leq t \leq 60$ ms). This means that the combustion downstream of the obstacle occurs in two times in Run B and in one time in Run A.

In the laminar case (Run B) the flame propagation is slower than in the test case (Run A). As a consequence, in Run B the venting rate towards the exit, promoted by the pressure gradient associated to the flame propagation, is comparable to the combustion rate. Then, as in the early combustion phase, the venting has the time to act, thus giving rise to the fourth overpressure peak when the flame is still propagating inside the channel (Figure 1 and Figure 2, Run B, $t = 46.5$ ms).

When the flame exits from the chamber and the *external explosion* blocks the venting, unburnt mixture remains accumulated behind the obstacle (Figure 2, Run B, $t = 49$ ms). Compared to the test case (Figure 2, Run A, $t = 40$ ms), in the laminar case a larger isolated region of reactants is formed due to the different times and locations of the reconnection of the two opposite flames passing around the obstacle (Figure 2, Run B, $t = 49$ ms). However, in Run B the *over-combustion* takes place without the turbulence effects on the reaction rate (Figure 2, Run B, $49 \leq t \leq 60$ ms), thus leading to a fifth peak that is lower and smoother than the corresponding peak in Run A (Figure 1).

In absence of the obstacle (Run C), a behaviour that lies between those of Run A and Run B can be observed (Figure 1). In Run C the flame propagation is faster than in Run B (the coupling between combustion and turbulent flow field is taken into account), but it is still slower than in Run A (there is no jetting flame and the turbulence generated is at a lower level). In Run D the flame propagation is slower compared to all the other cases simulated.

Consequently, also in Run C and Run D one peak more than Run A is found during the propagation inside the chamber (Figure 1 and Figure 2, Run C at $t = 42$ ms, Run D at $t = 47$ ms). In Run C this peak is higher than the fourth peak observed in Run B, on the contrary in Run D it is lower (Figure 1).

Moreover, also in Run C and Run D when the flame explodes outside the chamber, thus strongly reducing the venting rate, the combustion inside the chamber is not complete with almost the same regions of unburnt mixture accumulated along the chamber's walls (Figure 2, Run C at $t = 44$ ms, Run D at $t = 55$ ms). The *over-combustion* of this mixture causes the fifth overpressure peak (Figure 1 and Figure 2, Run C at $t = 46.6$ ms, Run D at $t = 60$ ms).

In both Run C and Run D this peak is lower than the fourth peak in Run A (Figure 1). Furthermore, in Run C it is sharper but comparable in intensity with the fifth peak in Run B (Figure 1). This is due to the fact that in Run C the combustion occurs in turbulent conditions, but it involves a less amount of reactants (Figure 2, Run C, $44 \leq t \leq 48$ ms) than Run B (Figure 2, Run B, $49 \leq t \leq 60$ ms).

Finally, Run D results again in a fifth peak lower than both, Run B and Run C (Figure 1). This occurs because of the slower flame propagation compared to Run B and Run C, and also due to the less amount of reactive mixture involved in the *over-combustion* (Figure 2, Run D, $49 \leq t \leq 60$ ms) than Run B (Figure 2, Run B, $55 \leq t \leq 70$ ms).

4. Conclusions

In the present work a validated LES-based model was adopted to study the unsteady propagation of stoichiometric CH_4/air premixed flame around an obstacle in a vented chamber starting from quiescent conditions. The model was coupled to a sub-grid combustion model able to follow all the stages of flame propagation, from laminar to fully turbulent. Simulations were also run by assuming the flame speed equal to the laminar value during all the propagation time, by eliminating the obstruction in the chamber, and by assuming laminar propagation in the empty chamber.

The comparison of the results obtained shows that the competition between combustion rate and venting rate is the main mechanism responsible for the overpressure peaks. Combustion rate is affected by the obstacle-induced turbulent flow field, which enhances the flame speed. Venting rate is affected by the pressure gradient generated by the flame propagation. However, when the flame propagation is very fast the increasing pressure level does not have the time to allow venting of the gas toward the chamber exit and, then, the overpressure increases rapidly. In the slower flame propagation (i.e., in absence of the obstacle and/or of the flame-turbulence interaction) venting has the time to occur thus emptying the combustion chamber and, then, giving rise to periodic and lower overpressure peaks.

5. References

- Boger, M., D. Veynante, H. Boughanem and A. Trouvé, 1998, Proc. Combust. Institute 27, 917.
- Charlette, F., C. Meneveau and D. Veynante, 2002, Combust. Flame 131(1/2), 159.
- Di Sarli, V., A. Di Benedetto and G. Russo, Proc. Int. Symp. Loss. Prev. and Safety Prom. Proc. Ind., Edinburgh, UK, 2007.
- Ibrahim, S.S., G.K. Hargrave and T.C. Williams, 2001, Exp. Thermal Fluid Sci. 24, 99.
- Jarvis, S. and G.K. Hargrave, 2006, Meas. Sci. Technol. 17, 91.
- Hargrave, G.K., S. Jarvis and T.C. Williams, 2002, Meas. Sci. Technol. 13, 1036.
- Kirkpatrick, M.P., S.W. Armfield, A.R. Masri and S.S. Ibrahim, 2003, Flow, Turbulence Combust. 70, 1.
- Lilly, D.K., 1992, Phys. Fluids, 4, 633.
- Lindstedt, R.P. and V. Sakthitharan, 1998, Combust. Flame 114, 469.
- Meneveau, C. and T. Poinso, 1991, Combust. Flame 86, 311.
- Naamansen, P., D. Baraldi, B.H. Hjertager, T. Solberg and R.S. Cant, 2002, J. Loss Prev. Process Ind. 15, 189.
- Patel, S.N.D.H., S.S. Ibrahim, M.A. Yehia and G.K. Hargrave, 2003, Exp. Thermal Fluid Sci. 27, 355.